Inhomogeneity correction for magnetic resonance images with fuzzy C-mean algorithm

Xiang Li*, Lihong Li, Hongbing Lu, Dongqing Chen, and Zengrong Liang
Department of Radiology, State University of New York at Stony Brook, USA

Abstract: Segmentation of magnetic resonance (MR) images plays an important role in quantitative analysis of brain tissue morphology and pathology. However, the inherent effect of image-intensity inhomogeneity renders a challenging problem and must be considered in any segmentation method. For example, the adaptive fuzzy c-mean (AFCM) image segmentation algorithm proposed by Pham and Prince can provide very good results in the presence of the inhomogeneity effect under the condition of low noise levels. Their results deteriorate quickly as the noise level goes up. In this paper, we present a new fuzzy segmentation algorithm to improve the noise performance of the AFCM algorithm. It achieves accurate segmentation in the presence of inhomogeneity effect and high noise levels by incorporating the spatial neighborhood information into the objective function. This new algorithm was tested by both simulated experimental and real clinical MR images. The results demonstrated the improved performance of this new algorithm over the AFCM in the clinical environment where the inhomogeneity and noise levels are commonly encountered.

Keywords: Fuzzy segmentation, Intensity inhomogeneity correction, Bias field, Magnetic Resonance Imaging.

I. Introduction

Magnetic Resonance Imaging (MRI) has several advantages over other medical imaging modalities -- high contrast between different soft tissues and high spatial resolution across the entire body field of view (FOV), so it has been widely used in clinical practice, especially in brain studies. Quantitative volumetric measurement and three-dimensional (3D) visualization of the brain tissues are very helpful to detect pathology, for example, multiple sclerosis (MS) disease. For this quantitative purpose, image segmentation plays an important role. A variety of intensity-based segmentation methods [1-4] have been proposed and have archived a noticeable success in the absence of image-intensity inhomogeneity effect. However, the intensity inhomogeneity effect, which is mainly due to the non-uniformity in the radio frequency (RF) field during data acquisition [5-7], results in the shading effect and renders a very challenging task for the image segmentation. The shading effect can cause severe errors when an intensity-based segmentation method is applied to the MR images corrupted by intensity inhomogeneity. It is well known that the inhomogeneity effect is multiple, which is also called as bias field.

Many of inhomogeneity correction methods have been reported in the literature. Dawant, *et al.* [8] manually selected some reference points within the image, and then reconstructed the bias field with the spline surface fitting technique. The selection of the reference points strongly depends on the user's experience and is time consuming for a large dataset. Some researchers [9-11] have adopted the homomorphic filtering to correct the inhomogeneity effect. This kind of methods is fast and easy to implement, but sometimes it will distort the image other than correct for it. Volurka, *et al.* [12] used the local gradient information in the image to estimate the bias field. Their results are sensitive to the estimation of both the image noise variance and the threshold to detect a boundary. Sled, *et al.* [13] assumed the probability density distribution of bias field as a Gaussian function with mean of 1, and estimated the corrected image by deconvoluting the bias field from the observed image. Their Gaussian assumption was not validated and the deconvolution is sensitive to the noise. Lee and Vannier [14] proposed an extended fuzzy C-mean clustering algorithm (FCM) to estimate the bias field. In their method, the image was classified into two classes: background and non-background. Each single mean of non-background class was replaced by the local mean in their method. The local mean could be a good estimate of the bias field, but contains noticeable error around edges. All of these methods can be considered as a straightforward approach.

Another type of approach is to correct for the inhomogeneity effect when segmenting the image and is called as simultaneous approach. Wells, *et al.* [15] proposed a Markov Random Field - Expectation Maximization (MRF-EM)

* xli@clio.rad.sunysb.edu; phone 631-4442736

algorithm to estimate the maximum *a posterior* probability (MAP) solution on the bias field, given the observed image. Their method needs manual selection of training samples to model the distribution of each class. Guillemaud and Brady [16] further refined this method by introducing an extra class, but the manual manner remains. Pham, *et al.* [17-18] proposed an unsupervised method, called an adaptive fuzzy C-mean (AFCM) algorithm, which can provide very good results in the presence of the inhomogeneity under the condition of low noise levels, as demonstrated by their simulation studies. However, its performance deteriorates quickly as the noise goes up, as shown in this paper. For most clinical studies, where a 1.5 Tesla or lower field strength whole body MRI systems are commonly used, the noise levels are relatively high, therefore, the AFCM algorithm must be improved for these clinical applications. The objective of this paper is to improve its noise performance by taking into account the spatial neighborhood information for the noise control, while keeping its adaptive advantage.

II. Methods

A. Standard FCM Algorithm

The standard fuzzy C-mean (FCM) algorithm is expressed as the minimization of the following objective function with respect to the membership function u and the centroid υ of each class:

$$J = \sum_{i=1}^{N} \sum_{k=1}^{C} u_{ik}^{p} \left\| y_i - \upsilon_k \right\|^2 \tag{1}$$

where u_{ik} is the membership value at voxel i for class k, such that $\sum_{k=1}^{C} u_{ik} = 1$, and C and N are the total numbers of classes and voxels, respectively. Index p reflects the weighting fractions among the fuzzy membership (to be discussed later). Notation y_i stands for the observed image intensity value at voxel i, and υ_k is the centroid of class k. The operator $\left\| \cdot \right\|$ can be any type of inner product norm in R^n. Typically the Euclidean norm is used. In the rest of this paper we will also adopt this norm definition. Usually, the weighting fraction index p is constrained to be larger than one. When p=1, the FCM algorithm reduces to fuzzy ISODATA algorithm [19]. When p is larger than one, it is guaranteed that the minimization process of above objective function can converge to local minimum [19-20]. Obviously, the objection function of equation (1) is minimized when each voxel, whose intensity is closer to the centroid of a particular class, is assigned a membership value with a higher probability, otherwise it is assigned a membership value of lower probability when its intensity is far from that centroid.

B. Adaptive FCM Algorithm

The standard FCM algorithm does not work well for images corrupted by intensity inhomogeneity and noise. So the AFCM algorithm was proposed by Pham, *et al.* [17-18] to improve the performance in a more realistic situation. The inhomogeneity effect was taken into account in their modified objective function:

$$J = \sum_{i=1}^{N} \sum_{k=1}^{C} u_{ik}^{p} \left\| y_i - \beta_i . \upsilon_k \right\|^2 + \lambda_1 \sum_{i=1}^{N} \sum_{j=1}^{R} (D_j * \beta)_i^2 + \lambda_2 \sum_{i=1}^{N} \sum_{j=1}^{R} \sum_{r=1}^{R} (D_j * D_r * \beta)_i^2 \tag{2}$$

where β is the bias field. For 2D situation, R equals to 2 or 3 while 3D application was used. Notations D_j and D_r are the standard forward finite difference operators along the different directions. The symbol * denotes the 1D discrete convolution operators. The first-order regularization term penalizes mainly the large variation in the bias field and the second-order regularization term penalizes mostly the discontinuities in the bias field. The parameter λ_1 and λ_2 control the first- and second-order regularization terms of the bias field. As Pham, *et al* mentioned that, without these two regularization terms, the bias field could always be found by minimizing the objective function, but the results would not be satisfactory. The parameter λ_1 and λ_2 should be set according to the magnitude of the intensity inhomogeneity in the image. If the parameter λ_1 and λ_2 were very large, the adaptive FCM algorithm would be reduced to the standard FCM.

For images of low noise levels, the AFCM algorithm can generate very good results in the presence of the inhomogeneity effect across the FOV. However, as mentioned in Pham's paper, when the images get noisier, this method may perform poorly. For many clinical studies, where a heavily weighted T_1 and T_2, FLAIR, diffusion, and/or perfusion images may be needed, the images from the commonly used 1.5 Tesla whole body MRI scanners are quite noisy. Therefore, the noise performance of the AFCM must be improved for these clinical studies. To that end, we propose the following modification on the AFCM algorithm.

C. Our Modified AFCM Algorithm

It is well known that the MRF-based segmentation methods perform very well under very noisy situations, because the labeling of each voxel is determined by both of its own statistics and its immediate neighborhood. Based on this observation, the AFCM algorithm is modified to incorporate the immediate neighborhood for an improved noise performance:

$$J = \sum_{n=1}^{S}\sum_{i=1}^{N}\sum_{k=1}^{C} u_{ik}^{p}\left\|y_{ni} - \beta_{ni}.\upsilon_{nk}\right\|^2 + \frac{\alpha}{N_R}\sum_{n=1}^{S}\sum_{i=1}^{N}\sum_{k=1}^{C} u_{ik}^{p}\sum_{r\in N_i}\left\|y_{nr} - \beta_{nr}.\upsilon_{nk}\right\|^2 + \lambda_1\sum_{n=1}^{S}\sum_{i=1}^{N}\sum_{j=1}^{R}(D_j * \beta_n)_i^2 + \lambda_2\sum_{n=1}^{S}\sum_{i=1}^{N}\sum_{j=1}^{R}\sum_{k=1}^{R}(D_j * D_k * \beta_n)_i^2 \quad (3)$$

where we have introduced four new notations into our modified AFCM objective function above. The first one is α, which is a weighting parameter for the neighborhood information of current voxel *i*. The second one is the N_R, which is the number of voxels within the neighborhood of voxel *i*. The third one is *S*, which represents the number of images. Therefore, the above equation can deal with the multispectral situation. For example, if we use T_1 and T_2 images together to perform the segmentation, *S* should be 2. The last one is N_i, which represents the neighborhood system of voxel *i*. Figure 1 is an example of the neighborhood system in two- and three dimensions, where N_R is 8 or 6. It is noted that we have assumed that different images have different bias field maps. This is often the case.

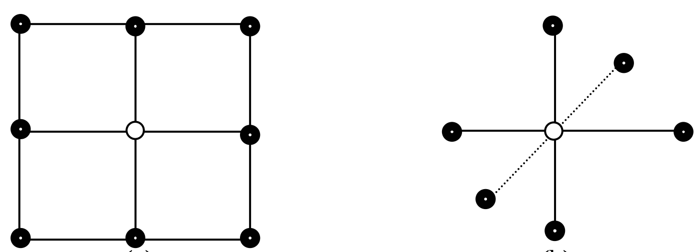

(a) (b)

Figure 1: An example of 2D (a) and 3D (b) neighborhood system, where the central empty circle represents the current pixel *i*, and its immediate neighboring pixels are those black solid dots.

The new objective function of equation (3) can be minimized in a similar way as the AFCM algorithm does for its cost function of equation (2). Since these objective functions are not global convex, the global minimum is usually not reachable. However, a reasonable local minimum can be easily obtained by taking the first derivatives of the objective function *J* with respect to the membership u_{ik}, centroid υ_{kn} and bias field β_{ni} and then setting these derivatives to zero. The following section will present the derivation for three equations to estimate the parameters for a local minimum of equation (3). In section III, we will show that the segmentation results obtained by the local minimum are very satisfactory.

(C.1). *Membership estimation*

The first partial derivative of the objective function *J* with respect to the membership u_{ik} should be zero, given the normalization condition on the membership $\sum_{k=1}^{C} u_{ik} = 1$. Therefore, we have to add a term of Lagrange multiplier to the objective function for the minimization as seen equation (4). Since the regularization terms on the bias field are irrelevant to the membership u_{ik}, so they have been eliminated from this equation:

$$J = \sum_{n=1}^{S}\sum_{i=1}^{N}\sum_{k=1}^{C} u_{ik}^{p}\left\|y_{ni} - \beta_{ni}.\upsilon_{nk}\right\|^2 + \frac{\alpha}{NR}\sum_{n=1}^{S}\sum_{i=1}^{N}\sum_{k=1}^{C} u_{ik}^{p}\sum_{r\in N_i}\left\|y_{nr} - \beta_{nr}\upsilon_{nk}\right\|^2) + \sum_{i=1}^{N}\lambda_i(1 - \sum_{k=1}^{C} u_{ik}) \quad (4)$$

Taking the partial derivative with respect to the membership u_{ik} and setting it to be zero, we get the following equation:

$$u_{ik} = \left(\frac{\lambda_i}{p\sum_{n=1}^{S}\left(\left\|y_{ni}-\beta_{ni}.\upsilon_{nk}\right\|^2+\frac{\alpha}{N_R}\sum_{r\in N_i}\left\|y_{nr}-\beta_{nr}.\upsilon_{nk}\right\|^2\right)}\right)^{\frac{1}{p-1}} \tag{5}$$

Since $\sum_{j=1}^{C} u_{ij} = 1$ for every i, then λ_i can be calculated by substituting u_{ik} into this constrain equation and is given by

$$\lambda_i = \frac{p}{\left(\sum_{j=1}^{C}\left(\sum_{n=1}^{S}\left(\left\|y_{ni}-\beta_{ni}.\upsilon_{nj}\right\|^2+\frac{\alpha}{N_R}\sum_{r\in N_i}\left\|y_{nr}-\beta_{nr}.\upsilon_{nj}\right\|^2\right)\right)^{-\frac{1}{p-1}}\right)^{p-1}} \tag{6}$$

Substituting λ_i back into equation (5) results in the estimation of the membership u_{ik}:

$$u_{ik} = \frac{\left(\sum_{n=1}^{S}\left(\left\|y_{ni}-\beta_{ni}.\upsilon_{nk}\right\|^2+\frac{\alpha}{N_R}\sum_{r\in N_i}\left\|y_r-\beta_r\upsilon_k\right\|^2\right)\right)^{-\frac{1}{p-1}}}{\sum_{j=1}^{C}\sum_{n=1}^{S}\left(\left\|y_{ni}-\beta_{ni}.\upsilon_{nj}\right\|^2+\frac{\alpha}{N_R}\sum_{r\in N_i}\left\|y_{nr}-\beta_{nr}.\upsilon_{nj}\right\|^2\right)^{-\frac{1}{p-1}}} \tag{7}$$

(C.2). ***Centroid estimation***

As mentioned before, the Eucledian distance was defined as a norm product in this paper. Therefore, taking the first partial derivative of the objective function J in equation (3) with respect to the centroid υ_{nk} of class k from image n and setting it to zero shall lead to the following equation:

$$\sum_{i=1}^{N} u_{ik}^p \beta_{ni}(y_{ni}-\beta_{ni}.\upsilon_{nk}) + \frac{\alpha}{N_R}\sum_{i=1}^{N} u_{ik}^p \sum_{r\in N_i}\beta_{nr}(y_{nr}-\beta_{nr}.\upsilon_{nk}) = 0 \tag{8}$$

By rearranging equation (8) we can have:

$$\upsilon_{nk} = \frac{\sum_{i=1}^{N} u_{ik}^p\left(\beta_{ni}y_{ni}+\frac{\alpha}{N_R}\sum_{r\in N_i}\beta_{nr}y_{nr}\right)}{\sum_{i=1}^{N} u_{ik}^p\left(\beta_{ni}^2+\frac{\alpha}{N_R}\sum_{r\in N_i}\beta_{nr}^2\right)} \tag{9}$$

(C.3). ***Bias field estimation***

In a similar way, taking the first partial derivative of the objective function J in equation (3) with respect to the bias field β_{ni} and setting it to be zero shall result in the following equation:

$$-\sum_{k=1}^{C} u_{ik}^p \upsilon_{nk}(y_{ni}-\beta_{ni}\upsilon_{nk}) - \frac{\alpha}{N_R}\sum_{k=1}^{C}\upsilon_{nk}(y_{ni}-\beta_{ni}\upsilon_{nk})\sum_{r\in N_i} u_{rk}^p + \lambda_1(\beta_n ** H_1)_i + \lambda_2(\beta_n ** H_2)_i = 0 \tag{10}$$

where we have adopted the same matrices H_1 and H_2 from the Pham's paper, which are defined as following for 2D study (for 3-D situation, it became more complex as seen in reference 19):

$$H_1 = \begin{bmatrix} 0 & -1 & 0 \\ -1 & 4 & -1 \\ 0 & -1 & 0 \end{bmatrix}, \quad H_2 = \begin{bmatrix} 0 & 0 & 1 & 0 & 0 \\ 0 & 2 & -8 & 2 & 0 \\ 1 & -8 & 20 & -8 & 1 \\ 0 & 2 & -8 & 2 & 0 \\ 0 & 0 & 1 & 0 & 0 \end{bmatrix}. \tag{11}$$

Rearranging this equation, we obtain equation (12):

$$\sum_{k=1}^{C}\upsilon_{nk}y_{ni}(u_{ik}^{p}+\frac{\alpha}{N_R}\sum_{r\in N_i}u_{rk}^{p})=\beta_{ni}.\sum_{k=1}^{C}\upsilon_{nk}^{2}(u_{ik}^{p}+\frac{\alpha}{N_R}\sum_{r\in N_i}u_{rk}^{p})+\lambda_1(\beta_n **H_1)_i+\lambda_2(\beta_n **H_2)_i\,. \quad (12)$$

It is very difficult to calculate the bias field β from equation (12). To mitigate this difficulty, the Jacobi scheme [21] is used to solve this equation. A brief review of the Jacobi iteration method is given below. Equation (12) can be rewritten in terms of a matrix mode:

$$B = W\beta_n + (\lambda_1 C_1 + \lambda_2 C_2)\beta_n = (W + C)\beta_n = A\beta_n \quad (13)$$

where B, β_n are the vectors with elements of $\sum_{k=1}^{C}\upsilon_{nk}y_{ni}(u_{ik}^{p}+\frac{\alpha}{N_R}\sum_{r\in N_i}u_{rk}^{p})$ and β_{ni}, respectively, and W is a diagonal matrix with the elements of $\sum_{k=1}^{C}\upsilon_{nk}^{2}(u_{ik}^{p}+\frac{\alpha}{N_R}\sum_{r\in N_i}u_{rk}^{p})$. Notations $C_1\beta_n$ and $C_2\beta_n$ are matrix expressions of $H_1 **\beta_n$ and $H_2 **\beta_n$, respectively, and $A = W + C = W + \lambda_1 C_1 + \lambda_2 C_2$.

If the matrix A is decomposed such that $A = D - L - U$, where D, L, U are the diagonal, lower triangular and upper triangular matrix, respectively, then the bias field β can be solved by the Jacobi iterations:

$$\beta_n^{i+1} = [(1-\omega)I + \omega D^{-1}(L+U)]\beta_n^{i} + \omega D^{-1}B \quad (14)$$

where ω is a weighting parameter and I is the identity matrix.

Usually, at least several hundreds (the number of image size) iterations are needed to achieve the convergence, which is very time consuming. The multi-grid strategy provides a natural way to reduce the computing effort and was used in this paper. Detailed description of the multi-grid algorithm can be found in the works [17-18, 21-22].

In summary, the new algorithm with simultaneous inhomogeneity correction and image segmentation, as well as consideration of spatial neighborhood membership for improved noise performance can be expressed as the followings:

1. Estimate the initial value of the centroid υ_{nk} for each class and set the bias field $\{\beta_{ni}\}_{i=1}^{N}$ equal to one for all voxels. Here, we adopted vector quantization method[24] to automatically get initial centroid υ_{nk}.
2. Compute the membership u_{ik} of the voxel belonging to each class using equation (7).
3. Calculate the new centroids υ_{nk} for each class based on equation (9).
4. Estimate the bias field using the Jacobi iterative scheme with multi-grid scheme to solve equation (12). For a 256x256x154 volume dataset, the Jacobi scheme with the multi-grid strategy always converges to a stable solution within 20 seconds on a PC Pentium IV with 2.6 GMHz CPU speed.
5. Update the membership u_{ik} for each voxel by equation (7). If the updated membership satisfies the termination criterion of equation (15) below, then the updated membership $\{u_{ik}\}$ and bias field $\{\beta_{ni}\}_{i=1}^{N}$ are saved as the final results. Otherwise, go to steps 3 and 4.

Termination of any iterative process is a common problem and has been a research topic for many years in the area of developing iterative algorithms for various applications. An empirical, yet commonly used termination criterion is written as:

$$Max(u_{ik}^{j+1} - u_{ik}^{j}) \le \varepsilon\,. \quad (15)$$

When the difference between membership u_{ik} at $(j+1)$-th iteration and at j-th iteration is less than the threshold ε as specified by the user, the iteration process terminates. The setting of the threshold is somewhat arbitrary. In most cases, a one percent is a good choice. Therefore, in this paper, the threshold ε was set to be 0.01.

III. Results

As a common practice, the presented new method above was tested first by computer simulation studies with comparison to the AFCM algorithm by controlled noise levels. For lower noise levels, i.e., from noise-free to nearly noise-free cases, the new method shall work very well as the AFCM did, as presented in the article of Pham, *et al.* [17-18]. For higher noise levels, an improved performance is expected. After the simulation studies, both the algorithms were further compared by digital phantom and clinical image datasets.

A. Computer Simulation Studies

Figure 2(a) shows the simulated strip image with a noticeable inhomogeneity effect. The intensities of the black and white vertical strips were 80 and 110, respectively, before the inhomogeneity effect was imposed. The image size is 256 by 256. The bias field is given by the following equation:

$$\beta_{ij} = 1 + 0.16\sin(2\pi j / 128) \quad (16)$$

i.e., the bias field is a sin wave along the vertical direction. Then the intensity of the black strip varies by 80 β_{ij} and the white strip by 110 β_{ij}, i.e., a 16% variation.

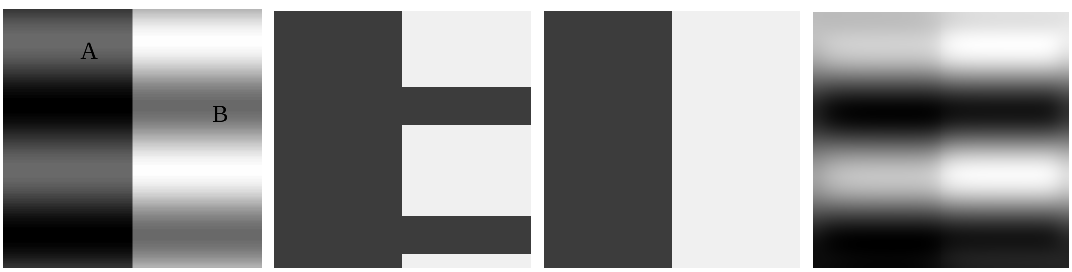

(a) (b) (c) (d)

Figure 2: Comparison of segmentation results without noise. (a) Simulated phantom strip image corrupted by sinusoid signal. (b) FCM segmentation without correction for the inhomogeneity. (c) AFCM and our segmentation results. (d) Estimated bias field by AFCM and our methods.

Figure 2(b) shows the segmentation of the standard FCM algorithm, an intensity-based method, from the phantom image without correction for the inhomogeneity effect. The severe error is clearly seen in the figure. Figure 2(c) is the segmentation result obtained by the AFCM and our method and Figure 2(d) is the bias field estimated by our method. Our method provides the same results as that of the AFCM, as expected for this noise-free experiment. Obviously, both AFCM and our method perform very well for correcting the inhomogeneity effect under the condition of noise-free. In Pham's paper, they mentioned that the algorithm is not sensitive to the parameters λ_1 and λ_2. This also is the case for our method as observed by many simulation trials. Actually when $\alpha = 0$, our method reduces to the AFCM algorithm. For all of the examples presented below, we will choose $\lambda_1 = 40000$, $\lambda_2 = 400000$ and $\alpha = 1.5$.

In order to evaluate the performance of the AFCM and our method in noisy situations, different noise levels were added to the phantom image of Figure 2(a). Figures 3(a), 3(e) and 3(i) show the simulated phantom images with 3%, 5% and 7% noise levels, respectively. Figures 3(b), 3(c) and 3(d) are the segmentation results from the 3% noise level data using the standard FCM, the AFCM and our method, respectively. The corresponding results from the 5% and 7% noise level data are shown by Figures 3(f), 3(g), and 3(h); 3(j),3(k) and 3(l), respectively. The noticeable inhomogeneity effect is seen again in the noisy cases in the FCM segmentation results of Figures 3(b), 3(f) and 3(j). The AFCM can compensate for the inhomogeneity effect to some degrees, but the results deteriorate as the noise level goes up, as seen in Figures 3(c) and 3(g). When noise level goes up to 7%, AFCM almost can not correct inhomogeneity effect. Our method performed consistently from noise-free up to 5% noise levels for accurate segmentation results. Even in very high noisy situation such as 7% noise level, there are just little artifacts in our segmentation results in Figure 3(l). Table 1 shows the quantitative results of segmentation ratio, which is defined as the ratio of the number of accurately labeled voxels over the number of whole voxels.

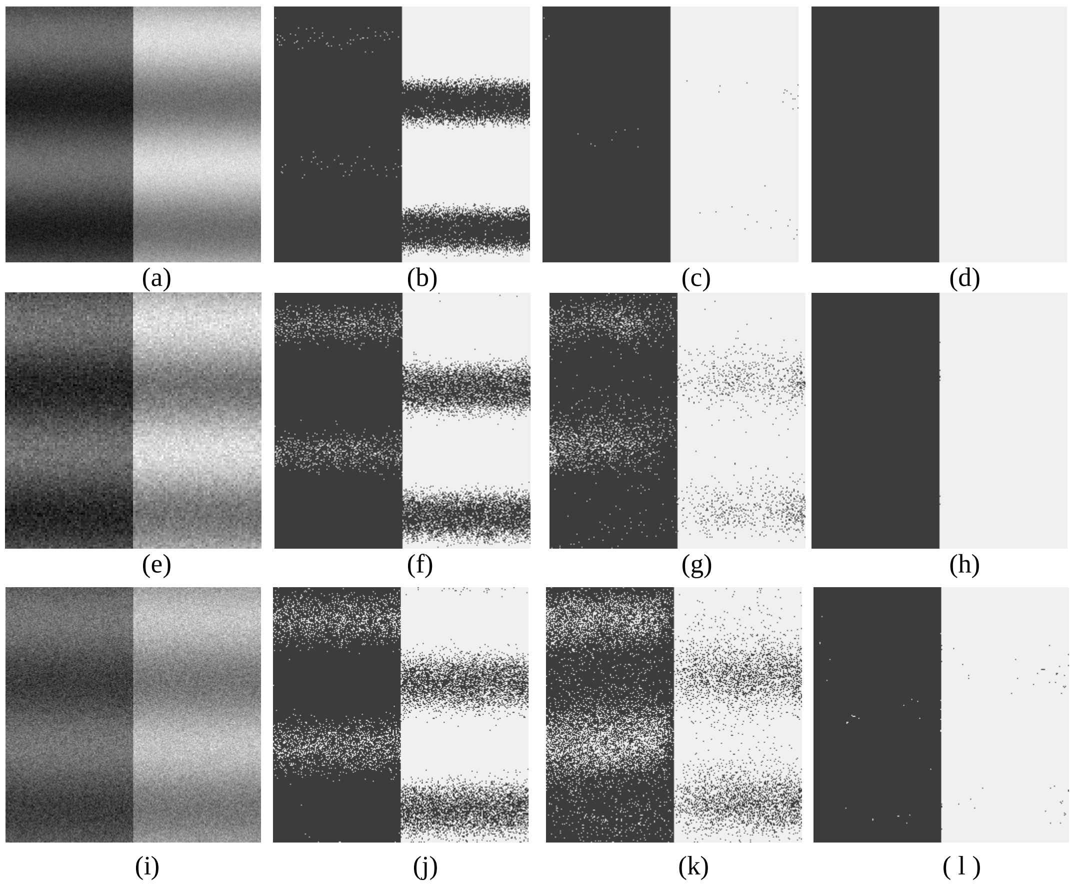

Figure3: Comparison of segmentation results based on different noise levels. From left to right for both rows: (a), (e) and (i) are the phantom images for 3%, 5% and 7% noise levels, respectively; (b), (f) and (j) are the FCM segmentations for the noise levels; (c), (g) and (k) are the AFCM segmentations; and (d), (h) and (l) are our segmentations.

Table 1: The quantitative comparison of accurate segmentation ratio between different segmentation methods

Noise ratio	FCM	AFCM	OURS
3%	87.23%	99.94%	100%
5%	86.72%	94.55%	99.99%
7%	85.53%	80.72%	99.86%

The above simulation studies agree with the AFCM results of Pham and Price, where they presented simulated phantom images with a lower noise level – nearly noise-free. It is seen that their results deteriorate quickly as the noise goes up. In the followings, we will further compare these two methods by real clinical data sets.

B. Digital Phantom Studies

Brain digital phantoms obtained from McConnell Brain Imaging Center of the Montreal Neurological Institute, McGill University were used to evaluate our method [23]. The advantage of using above digital phantom is that the phantom is very similar to real brain and has the ground truth to compare different segmentation method. First, we downloaded the ideal 3D T_1 and T_2 phantom images without noise and inhomogeneity effect. Here we added 4% noise and 40%, 60% inhomogeneity effect into the T_1 and T_2 phantom images as seen in figure4 (a) and figure 4(b), respectively. Thus, we compare our method and AFCM under two situations: 2D based on T1 image only and 3D multi-spectral (T_1 and T_2 images simultaneously).

Figure 4(c) is a ground truth. If conventional FCM segmentation method was applied to image corrupted by noise and inhomogeneity, there are severe errors as seen in Figure 4(d). First of all, we tried to segment image based on 2D T1 image only. Figure 4(e) and 4(f) show the final segmentation results by AFCM and our method, respectively. Obviously, these two methods can correct for inhomogeneity effect very well. However, there are too many artifacts in AFCM segmentation. Compared to AFCM, our method has a better performance under noisy situation by visual judgment. Secondly, we tried to use 3D T_1 and T_2 images together to perform the segmentation. Figure 4(g) and 4(h) show the segmentation results of AFCM and our method, respectively. Apparently, 3D multi-spectral scheme has better quality than just 2D study. Even in this situation, our method holds the better results than AFCM. In order to obtain the more objective and accurate comparison between AFCM and our method, quantitative analysis from several slices had been conducted. Table 2 shows the quantitative results of accurate segmentation ratio of different method based on the different situation. For 2D T_1 image study, the accuracy of our method is almost higher 4% than the AFCM. If we adopted 3D multi-spectral scheme, the accuracy of both methods dramatically increased. In this situation, our method also can obtain higher accuracy 2% than AFCM.

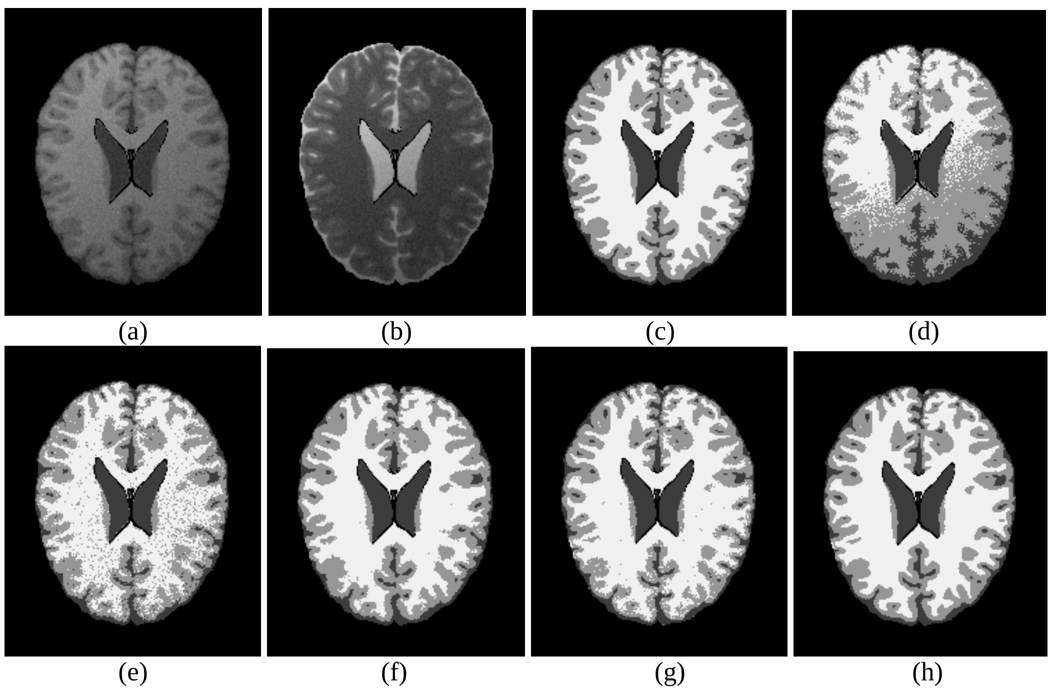

Figure 4: Digital phantom studies. (a) T_1 image. (b) T_2 image. (c) Ground truth. (d) FCM segmentation. (e) AFCM segmentation based on 2D T_1 image. (f) Ours segmentation based on 2D T_1 image. (g) AFCM segmentation using 3D multi-spectral data. (h) Ours segmentation using 3D multi-spectral data.

Figure 5 shows the 3D surface rendering of white matter (WM) based on different segmentation results from the same angle. Obviously, if inhomogeneity effect is not taken into account as seen in Figure 5(a), the part of WM segmented by FCM has been missed and some part, which is not belonging to WM, is also classified as WM. It is hard to see the real brain cortex, especially the convoluted sulci, in Figure 5(a). AFCM segmentation almost recovered the whole WM volume as seen in Figure 5(b). However, there are too many noises in the WM volume. Compared with FCM and AFCM algorithm, our method can correct inhomogeneity effect and keep the smooth surface of WM very well. The convoluted sulci can be clearly seen in Figure 5(c).

Table 2: Quantitative comparison of AFCM and our method

	2-D based on T1 only			3-D multi-spectral		
	FCM	AFCM	NEW	FCM	AFCM	NEW
Slice 75	0.6515	0.8510	0.8941	0.7263	0.9103	0.9415
Slice 95	0.6577	0.8839	0.9358	0.7293	0.9451	0.9658
Slice 115	0.7459	0.8781	0.9129	0.7588	0.9403	0.9583

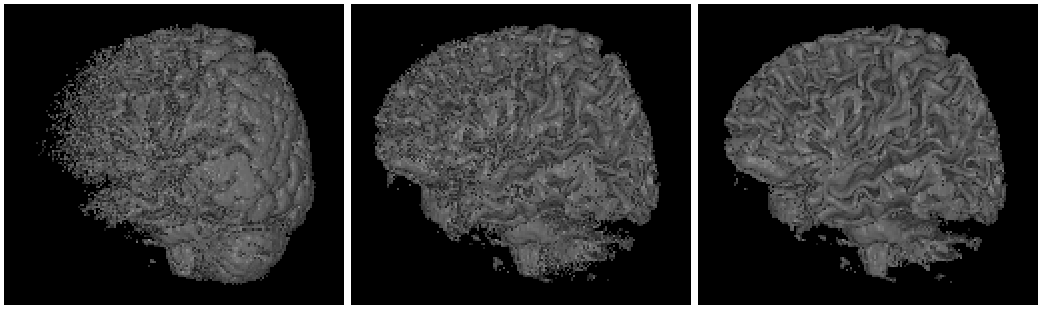

(a) (b) (c)

Figure5: 3D surface rendering. (a) FCM segmentation, (b) AFCM segmentation, (c) Ours segmentation.

C. Clinical Data Studies

MRI sessions were performed using a 1.5Tesla Marconi Edge whole-body scanner with a body coil as the transmitter and a birdcage head coil as the receiver. A 3D SPGR and 3D EXPRESS sequences were employed to acquire T_1 and T_2 weighted axial images covering the whole brain with 30^o flip angle, 1.5 mm slice thickness, 24 cm field-of-view (FOV), and 256x256 matrix size (0.9375 by 0.9375 mm). For the T_1 weighted image, T_R=50ms, T_E=5ms. For the T_2 weighted image, T_R=4000ms, T_E=95ms.

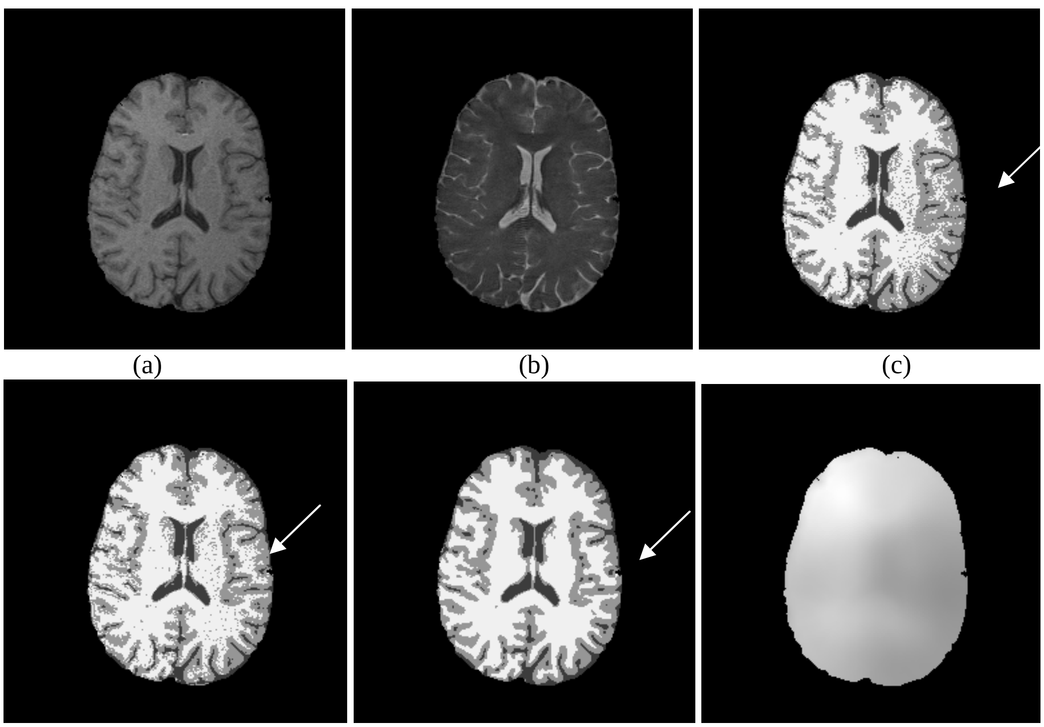

(a) (b) (c)

(d) (e) (f)

Figure 6: Clinical study. (a) T_1 image, (b) T_2 image, (c) FCM segmentation, (d) AFCM segmentation, (e) ours segmentation, (f) bias field estimated by new method.

First, we used vector quantization method to remove skull and scalp and get the initial centroids for each class. Here, the whole brain tissue was divided into three classes: WM, GM and CSF. Figures 6(a) and 6(d) show the one slice T_1 and T_2 image after preprocessing, respectively. All of the segmentation method based on the 3D multi-spectral data. There is no apparent inhomogeneity effect as seen in Figures 6(a) and 6(b). Figures 6(c), 6(d) and 6(e) show the segmentation results of FCM, AFCM and our method from same slice, respectively. It is clearly seen that both the noise and inhomogeneity deteriorate the FCM segmentation result. The central WM area contains many small spots, which shall not occur. The indicated region of interest (ROI) pointed by arrow shows error mainly due to the inhomogeneity effect. At this point, the AFCM can get better results than FCM. Most of WM can be accurately segmented seen in Figure 6(d). However, like FCM, there are too many artifacts in the AFCM segmentation result. It is clearly seen in Figure 6(e) that our method can correct inhomogeneity effect very well. Meanwhile, our method can obtain the very smooth segmentation result. Figure 6(f) shows the bias field estimated by our method. Unlike the phantom studies above, here we do not have the gold standard for comparison. All of the comparisons are just based on visual judgment.

IV. Discussion

From equation (3), it is clearly seen that the FCM and AFCM can be regarded as a special case of our method. When α is set to be zero, our method reduces to the exact AFCM algorithm. If bias field β is further confined to be 1, then the conventional FCM is obtained. Neighborhood information was introduced into FCM framework first by Ahmed *et al.*[20]. If there was no inhomogeneity effect, their method showed satisfactory performance. However, when it was applied to the images corrupted by inhomogeneity, their method did not work well. As a matter of fact, both Pham's work [17,18] and our experience show that the algorithm derived from equations (2) or (3) is not sensitive to the value of parameters λ_1 and λ_2 within a very large range. But this does not mean that parameters λ_1 and λ_2 can be set to any value. Too large λ_1 and λ_2 values result in too smooth bias field, which nearly equals to 1, and almost same result as FCM. On the other hand, if the value of λ_1 and λ_2 is too small even equals to zero, then very sharp bias field will be obtained. In this case, it is really hard to correct for inhomogeneity effect, which has a characteristic of smoothness. In this study, the fixed values of λ_1 and λ_2 as described in section III.A were suitable for all the cases analyzed in this paper.

It is well known that the bias field has a multiple characteristic. In so many literatures [13,15,16,20], the multiple bias field is transformed into additive through the logarithm transformation before performing the correction. Here, we prefer to hold the multiple property of bias field. Because logarithm transformation may alter the contrast and statistics property of the image, especially for the MRF-EM algorithm [15,16]. We know that each class in MR images has an approximated Gaussian distribution, which is not accurate after logarithm transformation. Therefore, it may cause some errors when performing segmentation and estimating the bias field. Based on above reason, straight multiple bias field could be a better choice than additive means after the logarithm transformation.

Our goal in this paper is to provide a more accurate segmentation for brain MR images. As a matter of fact, even for the high resolution MR images of Figure 6 (as seen in clinic), there are moderate noise and inhomogeneity inside. With the currently developed techniques, the inhomegeneity effect has been reduced dramatically, but it is impossible to eliminate this effect completely. It may not affect the human eyes, but will cause some errors of measurement and location when automatic intensity-based segmentation method is used. Therefore, if we want to get more accurate quantitative volume measurements of brain tissues, these two effects should be taken into account. That is why we devote a great effort to develop the new method which has shown a better performance than AFCM.

Of course, our method has some limitations. Above minimization process is a kind of conjugate gradient methods and cannot promise the global minimum, even though a lot of experiments have demonstrated that it always converges to a satisfactory result. Further theoretical researches are needed. The simulated annealing method or genetic algorithm may be the solution.

V. Conclusion

In this paper, a new inhomogeneity correction method for MR images has been proposed, which is based on AFCM and incorporates new constraint terms into the objective function. Simulated studies demonstrated that both AFCM and our new method work very well and have almost the same performances under condition of low noise levels. However, as the noise level goes up, the performance of AFCM becomes less satisfactory. Compared to AFCM, our new method is more robust even in the conditions of very noisy situation.

Acknowledgement

This work was supported in part by the National Institutes of Health (grant #CA82402) and the National Multiple Sclerosis Society (grant #RG3042-A-2).

References:

[1] J.C. Bezdeck, L.O. Hall, and L.P. Clarke, "Review of MR image segmentation techniques using pattern recognition", Medical Physics, vol.20, pp.1033-1048, 1993.

[2] Z. Liang, J.R. MacFall, and D.P. Harrington, "Parameter estimation and tissue segmentation from multispectral MR images", IEEE Trans. Medical Imaging, vol.13, pp.441-449, 1994.

[3] J.C. Rajapakse, J.N. Giedd, and J.L. Rapoport, "Statistical approach to segmentation of single channel cerebral MR images", IEEE Trans. Medical Imaging, vol.16, pp.176-186, 1997.

[4] Y. Zhang, M. Brady, and S. Smith, "Segmentation of brain MR images through a hidden markov random field model and expectation-maximization algorithm", IEEE Trans. Medical Imaging, vol.20, pp.45-57, 2001.

[5] B.R. Condon, J. Patterson, D. Wyper, A. Jenkins, and D.M. Hadley, "Image non-uniformity in magnetic resonance imaging: its magnitude and methods for its correction", Br. J. Radiology, vol.60, pp.83-87, 1987.

[6] T.K.F. Foo, C.E. Hayes, and Y.W. Kang, "Reduction of RF penetration effects in high field imaging", Magnetic Resonance in Medicine, vol.23, pp.287-301, 1992.

[7] L. Axel, J. Costantini, and J. Listerud, "Intensity correction in surface coil MR imaging", AJR, vol.148, pp.418-420, 1987.

[8] B.M. Dawant, A.P. Zijidenbos, and R.A. Margolin, "Correction of intensity variation in MR images for computer-aided tissue classification", IEEE Trans. Medical Imaging, vol.12, pp.770-781, 1993.

[9] B. Johnstion, M.S. Atkins, B. Mackiewich, and M. Anderson, "Segmentation of multiple sclerosis lesions in intensity corrected multispectral MRI", IEEE Trans. Medical Imaging, vol.15, pp.154-169, 1996.

[10] K.O. Lim and A. Pfefferbaum, "Segmentation of MR brain images into cerebrospinal fluid and white and gray matter", J. Comput. Assisted. Tomography, vol.13, pp.588-593, 1989.

[11] B.H. Brinkman, A. Manduca, and R.A. Robb, "Optimized homomorphic unsharp masking for MR grayscale inhomogeneity correction", IEEE Trans. Medical Imaging, vol.17, pp.161-171, 1998.

[12] E.A. Vokurka, N.A. Thacker, and A. Jackson, "A fast model independent method for automatic correction of intensity nonuniformity in MRI data", J. Magnetic Resonance Imaging, vol.10, pp.550-562, 1999.

[13] J.G. Sled, A.P. Zijidenbos, and A.C. Evans, "A nonparametric method for automatic correction of intensity nonuniformity in MRI data", IEEE Trans. Medical Imaging, vol.15, pp.87- 97, 1998.

[14] S.K. Lee and M.W. Vannier, "Post-acquisition correction of MR inhomogeneity", Magnetic Resonance in Medicine, vol.36, pp.275-286, 1996.

[15] W.M. Wells, III, W.E.L. Grimson, R.Kikinis, and F.A. Jolesz, "Adaptive segmentation of MRI data", IEEE Trans. Medical Imaging, vol.15, pp.429-442, 1996.

[16] R. Guillemaud and M. Brady, "Estimating the bias field of MR images", IEEE Trans. Medical Imaging, vol.16, pp.238-251, 1998.

[17] D.L. Pham and J.L. Prince, "An adaptive fuzzy C-means algorithm for image segmentation in the presence of intensity inhomogeneities", Pattern Recognition Letters. vol.20, pp.57-68, 1999.

[18] D.L. Pham and J.L. Prince, "Adaptive fuzzy segmentation of magnetic resonance images", IEEE Trans. Medical Imaging, vol.18, pp.737-752, 1999.

[19] J.C. Bezdek, "A convergence theorem for the fuzzy ISODATA clustering algorithms", IEEE Trans. Pattern Anal. And Machine Intell., vol.PAMI-2, pp.1-8, 1980.

[20] M.N. Ahmed, S.M. Yamany, N. Mohamed and A.A. Farag, "A modified fuzzy c-mean algorithm for bias field estimation and segmentation of MRI data", IEEE Trans. Medical Imaging, vol.21, pp.193-199, 2002.

[21] P. Wesseling, "An introduction to Multigrid methods", Wiley, New York, pp42, 1992.

[22] M. Unser, "Multigrid adaptive image processing", Proceedings of IEEE conference on image processing, vol.I, pp.49-52, 1995.

[23] C.A. Cocosco, V. Kollokian, R.K.-S. Kwan, A.C. Evans, "BrainWeb: Online interface to a 3D MRI simulated brain database", NeuroImage, vol.5, no.4, part 2/4, S425, 1997. http://www.bic.mni.mcgill.ca/brainweb/.

[24] D. Chen, L. Li, and Z. Liang, "A self-adaptive vector quantization algorithm for MR image segmentation", ISMRM, vol.1, pp.122, 1999.